Asymptotic Solutions for High Frequency Helmholtz Equations in Anisotropic Media with Hankel Functions

Matthew Jacobs & Songting Luo

Journal of Scientific Computing

ISSN 0885-7474 Volume 80 Number 2

J Sci Comput (2019) 80:808-833 DOI 10.1007/s10915-019-00957-8





Your article is protected by copyright and all rights are held exclusively by Springer Science+Business Media, LLC, part of **Springer Nature. This e-offprint is for personal** use only and shall not be self-archived in electronic repositories. If you wish to selfarchive your article, please use the accepted manuscript version for posting on your own website. You may further deposit the accepted manuscript version in any repository, provided it is only made publicly available 12 months after official publication or later and provided acknowledgement is given to the original source of publication and a link is inserted to the published article on Springer's website. The link must be accompanied by the following text: "The final publication is available at link.springer.com".



Journal of Scientific Computing (2019) 80:808–833 https://doi.org/10.1007/s10915-019-00957-8



Asymptotic Solutions for High Frequency Helmholtz Equations in Anisotropic Media with Hankel Functions

Matthew Jacobs 1 · Songting Luo1

Received: 9 April 2018 / Revised: 7 March 2019 / Accepted: 6 April 2019 / Published online: 13 April 2019 © Springer Science+Business Media, LLC, part of Springer Nature 2019

Abstract

We present asymptotic methods for solving high frequency Helmholtz equations in anisotropic media. The methods are motivated by Babich's expansion that uses Hankel functions of the first kind to approximate the solution of high frequency Helmholtz equation in isotropic media. Within Babich's expansion, we can derive the anisotropic eikonal equation and a recurrent system of transport equations to determine the phase and amplitude terms of the wave, respectively. In order to reconstruct the wave with the phase and amplitude terms for any high frequencies, they must be computed with high-order accuracy, for which a high-order factorization approach based on power series expansions at the primary source is applied first to resolve the source singularities, after that high-order schemes can be implemented efficiently. Rigorous formulations are derived, and numerical examples are presented to demonstrate the methods.

Keywords Anisotropic Helmholtz equation \cdot Asymptotic approximation \cdot Babich's expansion \cdot Anisotropic eikonal equation \cdot Source singularity \cdot High-order factorization \cdot High-order scheme

Mathematics Subject Classification 65N06 · 41A60

1 Introduction

We consider the Helmholtz equation in anisotropic media,

$$\nabla_{\mathbf{r}} \cdot \mathbf{A}(\mathbf{r}) \cdot \nabla_{\mathbf{r}} U(\mathbf{r}; \mathbf{r}_0) + \frac{\omega^2}{v^2} U(\mathbf{r}; \mathbf{r}_0) = -\delta(\mathbf{r} - \mathbf{r}_0), \ \mathbf{r} \in \mathbf{R}^d,$$
(1)

with Sommerfeld radiation condition at infinity, where d is the dimension, $\nabla_{\mathbf{r}}$ denotes the gradient at $\mathbf{r} \equiv (x, y, z)$, $\mathbf{r}_0 \equiv (x_0, y_0, z_0)$ is the primary source point, $U(\mathbf{r}; \mathbf{r}_0)$ is the

Matthew Jacobs jacobsm@iastate.edu

Department of Mathematics, Iowa State University, Ames, IA 50011, USA



wave, ω is the frequency, and $v(\mathbf{r})$ is the wave speed in the anisotropic medium that is characterized by a symmetric positive definite (SPD) tensor $A(\mathbf{r})$. If A is the identity tensor, the equation reduces to the isotropic case. The anisotropic Helmholtz equation (1) arises in various applications, ranging from acoustics, electromagnetics, elasticity to geophysics. It is therefore highly desirable to develop efficient and accurate numerical methods for solving this equation. The solution is highly oscillatory when the frequency ω is large. For example, in the isotropic case, denote $\lambda_{\min} = 2\pi v_{\min}/\omega$ as the smallest wavelength of the wave propagating in a bounded domain Ω , and let $k = \operatorname{diam}(\Omega)/\lambda_{\min}$ be the number of waves propagating in the domain Ω . For numerical methods based on direct discretization of the equation, such as finite-element and finite-difference methods, it is well known that the "pollution effect" (large dispersion error) in the finite-element method (e.g., piecewise linear finite-element method) is unavoidable for 2-dimensional (2D) and 3-dimensional (3D) Helmholtz equations in the pre-asymptotic regime $k^2h \gg 1$ if the wavenumber k is large [3], where h is the mesh size of the discretized problem. In order to avoid the pollution effect in finite-element methods for Helmholtz equations in the high frequency regime, one has to choose the mesh size hsatisfying $k^2h \ll 1$ [3]. In practice, this condition would exclude reliable wave computation in 3D applications for moderate and higher frequencies [3], in that the condition $k^2h \ll 1$ would imply that the dimension of the stiffness matrix of the discretized system is of order $O(h^{-3}) = O(k^6)$, and the discretized system of linear equations is highly indefinite such that the solution process becomes too expensive even for k in the range from 10 to 20. Therefore, alternative methods are sought to tackle this highly challenging high-frequency wave propagation problem.

We will investigate asymptotic approaches based on asymptotic high frequency theories [2,7,13], notably geometrical optics (GO). GO approximations have been developed for the isotropic case with $\bf A$ the identity tensor. In a GO approximation, instead of computing the wave directly, the phase and amplitude terms of the wave, which are assumed to be independent of the frequency ω , are computed and used to reconstruct the wave. Since the phase and amplitude terms are frequency-independent, they are not as oscillatory as the wave such that they can be computed more efficiently in general. Among a variety of GO approximations in the literature, there are two approximating approaches that are popularly applied in applications.

One asymptotic approach is based on the Wentzel-Kramers-Brillouin (WKB) approximation [7,13], with the wave approximated as

$$U(\mathbf{r}; \mathbf{r}_0) = e^{i\omega\tau(\mathbf{r}; \mathbf{r}_0)} \sum_{k=0}^{\infty} A_k(\mathbf{r}; \mathbf{r}_0) / (i\omega)^k, \text{ as } \omega \to \infty,$$
 (2)

where $\iota = \sqrt{-1}$, τ is the phase, and $\{A_k\}_{k=0}^{\infty}$ are the amplitude terms. By substituting the ansatz (2) into the Helmholtz equation (1) and collecting terms in the same order of ω , one can find that τ satisfies the eikonal equation,

$$|\nabla_{\mathbf{r}}\tau(\mathbf{r};\mathbf{r}_0)| = \frac{1}{v(\mathbf{r})}, \ \tau(\mathbf{r}_0;\mathbf{r}_0) = 0, \tag{3}$$

and $\{A_k\}_{k=0}^{\infty}$ satisfy a recurrent system,

$$A_{-1} \equiv 0,$$

$$2\nabla_{\mathbf{r}}\tau(\mathbf{r}; \mathbf{r}_{0}) \cdot \nabla_{\mathbf{r}}A_{k}(\mathbf{r}; \mathbf{r}_{0}) + \nabla_{\mathbf{r}}^{2}\tau(\mathbf{r}; \mathbf{r}_{0})A_{k}(\mathbf{r}; \mathbf{r}_{0}) = -\nabla_{\mathbf{r}}^{2}A_{k-1}(\mathbf{r}; \mathbf{r}_{0}), \ k \geq 0.$$
(4)

These equations are weakly coupled in the sense that the eikonal equation (3) needs to be solved first to provide necessary coefficients for the transport equation (4), and higher order



amplitude terms depend on lower order amplitude terms, but not vice versa. The eikonal equation is a first-order nonlinear partial differential equation (PDE), in general it does not have a globally defined classical solution. The concept of viscosity solution was introduced to pick a uniquely defined weak solution among many possible generalized solutions for such nonlinear first-order PDEs [5,6], and the viscosity solution of the eikonal equation is the so-called first-arrival traveltimes [14], which is continuous everywhere but not necessarily differentiable everywhere.

Another asymptotic approach is based on the Babich's expansion with Hankel functions [2], i.e.,

$$U(\mathbf{r}; \mathbf{r}_0) = \sum_{k=0}^{\infty} v_k(\mathbf{r}; \mathbf{r}_0) f_{k-(d-2)/2}(\omega, \tau(\mathbf{r}; \mathbf{r}_0)), \text{ as } \omega \to \infty,$$
 (5)

where τ is the phase that satisfies the eikonal equation (3), f_q ($q \equiv k - (d-2)/2$) is defined as

$$f_q(\omega, \tau(\mathbf{r}; \mathbf{r}_0)) = \iota \frac{\sqrt{\pi}}{2} e^{\iota q \pi} \left(\frac{2\tau(\mathbf{r}; \mathbf{r}_0)}{\omega} \right)^q H_q^{(1)}(\omega \tau(\mathbf{r}; \mathbf{r}_0)), \tag{6}$$

with $H_q^{(1)}$ the q-th Hankel function of first kind, and $\{v_k\}_{k=0}^{\infty}$ are the amplitude terms satisfying a recurrent system,

$$v_{-1} \equiv 0,$$

$$2\nabla_{\mathbf{r}}\tau^{2}(\mathbf{r}; \mathbf{r}_{0}) \cdot \nabla_{\mathbf{r}}v_{k}(\mathbf{r}; \mathbf{r}_{0}) + v_{k}(\mathbf{r}; \mathbf{r}_{0}) \left[\nabla_{\mathbf{r}}^{2}\tau^{2}(\mathbf{r}; \mathbf{r}_{0}) + \frac{2(2k+1-d)}{v^{2}(\mathbf{r})}\right]$$

$$= \nabla_{\mathbf{r}}^{2}v_{k-1}(\mathbf{r}; \mathbf{r}_{0}), \ k \geq 0.$$
(7)

These equations are weakly coupled, similarly as in the WKB approximation. Therefore they must be solved in a similar way.

High-order schemes for the eikonal and transport equations can be designed to compute the phase and amplitude terms such that the wave can be reconstructed for any high frequencies [4, 20,22,24,27-29]. The major difference between the WKB approximation (2) and the Babich's expansion (5) is that the later is more robust to achieve uniform accuracy near the source \mathbf{r}_0 [2,9,16–18].

Both the WKB approximation and the Babich's expansion have been applied successfully to numerically solve the Helmholtz equation (1) in the isotropic case [2,7,9,13,16–18,20, 22,24,27–29]. In order to implement these approaches numerically, the unbounded domain needs to be truncated such that the computation is performed on a bounded computational domain, and outgoing boundary conditions are assumed at the computational boundary. With these assumptions, efficient and accurate asymptotic numerical methods based on (2) and (5) have been successfully designed and implemented [20,22,24,27–29].

In this work, we further investigate the feasibility of the asymptotic approaches for solving the general anisotropic Helmholtz equation (1). We will focus on the Babich's expansion with Hankel functions of first kind. It turns out the phase and amplitude terms will satisfy similar equations as the eikonal equation (3) and the transport equations (7), respectively. Once the equations are derived, we will design efficient high-order numerical schemes to compute the phase and amplitude terms with high-order accuracy, such that they can be used to reconstruct the wave for any given high frequency ω .

The rest of the paper is organized as follows. In Sect. 2, we first present the formulations resulting from applying the Babich's expansion to the anisotropic Helmholtz equation, and



then we present high-order numerical schemes for solving the governing equations of the phase and amplitude terms, along with the factorization approach that can resolve the source singularities efficiently. In Sect. 3, numerical experiments are presented to demonstrate the performance of the methods. Concluding remarks are given in Sect. 4 along with a description of ongoing and future projects.

2 Asymptotic Methods for Anisotropic Helmholtz Equation

In this section, we first present the Babich's expansion for the anisotropic Helmholtz equation (1), following which we present the numerical schemes for solving the governing equations of the phase and amplitude terms. For notational simplicity, we derive the formulations in 2-dimensional (2D) spaces. Extension to higher dimensions is straightforward, which is presented in the Appendix. We assume the computational domain is $\Omega = [x_{\min}, x_{\max}] \times [z_{\min}, z_{\max}]$ (km), $\mathbf{r} = (x, z)$, $\mathbf{r}_0 = (x_0, z_0)$, $\nabla_{\mathbf{r}} = (\partial_x, \partial_z)$, and the anisotropic tensor is

$$\mathbf{A}(\mathbf{r}) \equiv \begin{pmatrix} a(\mathbf{r}) & -c(\mathbf{r}) \\ -c(\mathbf{r}) & b(\mathbf{r}) \end{pmatrix},$$

with a > 0, b > 0, $ab - c^2 > 0$.

2.1 Babich's Expansion

We apply the Babich's expansion (5) to the anisotropic Helmholtz equation (1), and derive the governing equations for the phase and amplitude terms. The governing equations for the phase and amplitude terms in the WKB expansion (2) can be derived similarly and are presented in the Appendix.

Theorem 1 In the Babich's expansion (5) for the anisotropic Helmholtz equation (1), the phase τ satisfies the anisotropic eikonal equation,

$$\sqrt{\nabla_r \tau(r; r_0) \cdot A(r) \cdot \nabla_r \tau(r; r_0)} = \frac{1}{v(r)}, \ \tau(r_0; r_0) = 0, \tag{8}$$

and the amplitude terms $\{v_k\}_{k=0}^{\infty}$ satisfy the following recurrent system,

$$v_{-1} \equiv 0,$$

$$(\beta T_x + \gamma T_z + 4(k-1)N + aT_{xx} - 2cT_{xz} + bT_{zz})v_k + 2\{(aT_x - cT_z)(v_k)_x + (bT_z - cT_x)(v_k)_z\}$$

$$= (\beta(v_{k-1})_x + \gamma(v_{k-1})_z) + (a(v_{k-1})_{xx} - 2c(v_{k-1})_{xz} + b(v_{k-1})_{zz}), \ k \ge 0,$$

$$(9)$$

where $\beta \equiv a_x - c_z$, $\gamma \equiv b_z - c_x$, $N \equiv 1/v^2$, and $T \equiv \tau^2$.

Theorem 1 can be proved with the following lemma.

Lemma 1 For the function f_k defined in (6) and rewritten as

$$f_k(z) = \frac{\iota\sqrt{\pi}}{2}e^{\iota k\pi} \frac{2^k}{\omega^{2k}} z^k H_k^{(1)}(z), \text{ with } z = \omega\tau,$$

we have

$$f'_k(z) = \frac{2kf_k(z)}{z} + \frac{\omega^2}{2z}f_{k+1}(z),$$



and

$$f_k''(z) = \left(\frac{4k^2 - 2k}{z^2} - 1\right) f_k(z) + \frac{(2k - 1)\omega^2}{2z^2} f_{k+1}(z).$$

Furthermore, we have

$$f_k(\omega \tau) = O\left(\frac{1}{\omega^{2k+1/2}}\right), \text{ as } \omega \to \infty.$$

Lemma 1 is an extension of the following properties of Hankel functions of first kind [1],

$$\begin{split} H_{k-1}^{(1)}(z) + H_{k+1}^{(1)}(z) &= \frac{2k}{z} H_k^{(1)}(z), \\ H_{k-1}^{(1)}(z) - H_{k+1}^{(1)}(z) &= 2H_k^{(1)'}(z), \\ H_k^{(1)'}(z) &= H_{k-1}^{(1)}(z) - \frac{k}{z} H_k^{(1)}(z), \\ H_k^{(1)'}(z) &= -H_{k+1}^{(1)}(z) + \frac{k}{z} H_k^{(1)}(z). \end{split}$$

With Lemma 1, we can show that

$$\begin{split} U_{x} &= \sum_{k=0}^{\infty} (v_{k})_{x} f_{k} - 2v_{k} \tau \tau_{x} f_{k-1}, \\ U_{z} &= \sum_{k=0}^{\infty} (v_{k})_{z} f_{k} - 2v_{k} \tau \tau_{z} f_{k-1}, \\ U_{xx} &= \sum_{k=0}^{\infty} (v_{k})_{xx} f_{k} - \omega^{2} v_{k} \tau_{x}^{2} f_{k} - \left(\frac{(v_{k})_{x} \tau_{x}}{\tau} + v_{k} \tau_{x}^{2} \frac{2k-1}{2\tau^{2}} + \frac{v_{k} \tau_{xx}}{2\tau} \right) 4\tau^{2} f_{k-1}, \\ U_{zz} &= \sum_{k=0}^{\infty} (v_{k})_{zz} f_{k} - \omega^{2} v_{k} \tau_{z}^{2} f_{k} - \left(\frac{(v_{k})_{z} \tau_{z}}{\tau} + v_{k} \tau_{z}^{2} \frac{2k-1}{2\tau^{2}} + \frac{v_{k} \tau_{zz}}{2\tau} \right) 4\tau^{2} f_{k-1}, \\ U_{xz} &= \sum_{k=0}^{\infty} (v_{k})_{xz} f_{k} - \omega^{2} v_{k} \tau_{x} \tau_{z} f_{k} \\ &- \left(\frac{(v_{k})_{x} \tau_{z}}{2\tau} + \frac{(v_{k})_{z} \tau_{x}}{2\tau} + v_{k} \tau_{x} \tau_{z} \frac{2k-1}{2\tau^{2}} + \frac{v_{k} \tau_{xz}}{2\tau} \right) 4\tau^{2} f_{k-1}. \end{split}$$

By substituting the above formulas into the anisotropic Helmholtz equation (1) in 2D, i.e.,

$$\beta U_x + \gamma U_z + aU_{xx} - 2cU_{xz} + bU_{zz} + \omega^2 NU = -\delta(\mathbf{r} - \mathbf{r}_0),$$

we have.

$$\sum_{k=0}^{\infty} \{ [\beta(v_k)_x + \gamma(v_k)_z] + [a(v_k)_{xx} - 2c(v_k)_{xz} + b(v_k)_{zz}] \} f_k$$

$$- (a\tau_x^2 - 2c\tau_x\tau_z + b\tau_z^2 - N)\omega^2 v_k f_k - 2(\beta\tau_x + \gamma\tau_z)\tau v_k f_{k-1}$$

$$- \left(a\frac{(v_k)_x\tau_x}{\tau} - c\frac{(v_k)_z\tau_x + (v_k)_x\tau_z}{\tau} + b\frac{(v_k)_z\tau_z}{\tau} \right) 4\tau^2 f_{k-1}$$

$$- (a\tau_x^2 - 2c\tau_x\tau_z + b\tau_z^2)2(2k-1)v_k f_{k-1}$$

$$- (a\tau_{xx} - 2c\tau_{xz} + b\tau_{zz})2\tau v_k f_{k-1} = -\delta(\mathbf{r} - \mathbf{r}_0).$$



By collecting the terms in the same order of ω as $\omega \to \infty$, we have

$$a\tau_x^2 - 2c\tau_x\tau_z + b\tau_z^2 = N \equiv 1/v^2,$$

which is the anisotropic eikonal equation (8) after taking the square root, and

$$2(\beta \tau_{x} + \gamma \tau_{z})\tau v_{k} + 2(2k - 1)Nv_{k} + (a\tau_{xx} - 2c\tau_{xz} + b\tau_{zz})2\tau v_{k}$$

$$+ \left(a\frac{(v_{k})_{x}\tau_{x}}{\tau} - c\frac{(v_{k})_{z}\tau_{x} + (v_{k})_{x}\tau_{z}}{\tau} + b\frac{(v_{k})_{z}\tau_{z}}{\tau}\right)4\tau^{2}$$

$$= [\beta(v_{k-1})_{x} + \gamma(v_{k-1})_{z}] + [a(v_{k-1})_{xx} - 2c(v_{k-1})_{xz} + b(v_{k-1})_{zz}],$$

which is the transport equation (9) after using

$$T = \tau^2$$
, $\nabla T = 2\tau \nabla \tau$, $T_{xx} = 2(\tau_x^2 + \tau \tau_{xx})$, $T_{zz} = 2(\tau_z^2 + \tau \tau_{zz})$, $T_{xz} = 2(\tau_x \tau_z + \tau \tau_{xz})$.

With the governing equations derived in Theorem 1, we can first solve the anisotropic eikonal equation (8) for τ , and then solve the recurrent system of transport equations (9) for $\{v_k\}_{k=0}^{\infty}$. The solutions are used to reconstruct the wave with the Babich's expansion (5) for any high frequencies ω . In order to approximate the wave faithfully, high-order accurate τ and $\{v_k\}_{k=0}^{\infty}$ must be computed. For instance, since second derivatives of the solutions are in the coefficients of the governing equations (9), in order to have first-order accurate v_1 , third-order accurate v_0 and fifth-order accurate τ are needed. The amplitude terms $\{v_k\}_{k=0}^{\infty}$ are smooth at the source, therefore, high-order schemes can be applied efficiently to compute them with high-order accuracy, provided that τ is given with required high-order accuracy. However, computing τ efficiently by high-order schemes with high-order accuracy is nontrivial due to the source singularities. We now present detailed procedures to resolve this issue.

2.2 High-Order Schemes for Governing Equations

We present efficient schemes for computing high-order accurate τ and $\{v_k\}_{k=0}^{\infty}$.

2.2.1 Factored Anisotropic Eikonal Equation

The main difficulty for solving the anisotropic eikonal equation (8) with high-order accuracy is the source singularities. In [21], a factorization approach was introduced to resolve the source singularities. Then efficient first-order schemes were designed to obtain clean first-order accuracy. The factorization approach follows the ideas that were developed to resolve the source singularities for the isotropic eikonal equation (3) [8,19,20,22–24,26–29,31]. Here, we extend the ideas to design high-order schemes for solving the anisotropic eikonal equation (8). In the factorization approach, τ is decomposed as

$$\tau(\mathbf{r}; \mathbf{r}_0) = \tilde{\tau}(\mathbf{r}; \mathbf{r}_0) u(\mathbf{r}; \mathbf{r}_0), \tag{10}$$

where $\tilde{\tau}$ is an analytical factor that captures the source singularities such that the other factor u serves as a smooth correction term at the source. Substituting (10) into the anisotropic eikonal equation (8) yields a factored anisotropic eikonal equation for u,

$$\sqrt{u^2 \nabla_{\mathbf{r}} \tilde{\tau} \cdot \mathbf{A} \cdot \nabla_{\mathbf{r}} \tilde{\tau} + \tilde{\tau}^2 \nabla_{\mathbf{r}} u \cdot \mathbf{A} \cdot \nabla_{\mathbf{r}} u + 2\tau u \nabla_{\mathbf{r}} \tilde{\tau} \cdot \mathbf{A} \cdot \nabla_{\mathbf{r}} u} = \frac{1}{v}.$$
 (11)

Since u is smooth at the source, the factored anisotropic eikonal equation (11) can be solved efficiently with high-order numerical methods to compute u with high-order accuracy. Then



 τ can be recovered with high-order accuracy through (10). In practice, for example, one may choose $\tilde{\tau}(\mathbf{r}; \mathbf{r}_0)$ to be the solution of the following anisotropic eikonal equation with constant coefficients [21], i.e.,

$$\sqrt{\nabla_{\mathbf{r}}\tilde{\tau}\cdot\mathbf{A}(\mathbf{r}_0)\cdot\nabla_{\mathbf{r}}\tilde{\tau}}=1/v(\mathbf{r}_0).$$

Then $u(\mathbf{r}_0; \mathbf{r}_0) = 1$, and $u(\mathbf{r}; \mathbf{r}_0) = \tau(\mathbf{r}; \mathbf{r}_0)/\tilde{\tau}(\mathbf{r}; \mathbf{r}_0)$ for $\mathbf{r} \neq \mathbf{r}_0$.

In general, $\tilde{\tau}$ can be derived in a systematic way near the source such that it fulfills any accuracy requirement in applications. Furthermore, the factored anisotropic eikonal equation (11) and the recurrent system of transport equations (9) need to be solved with high-order accuracy. In order to apply high-order schemes, the values of the solutions near the source need to be initialized with high-order accuracy. We present a systematic approach for computing $\tilde{\tau}$, based on high-order approximation near the source, in the following section.

2.2.2 High-Order Approximations of τ and $\{v_k\}_{k=0}^{\infty}$ Near r_0

We can compute high-order approximations of τ and $\{v_k\}_{k=0}^{\infty}$ near the source \mathbf{r}_0 using power series expansions, which was first introduced for the isotropic eikonal equation (3) [23]. Without loss of generality, we assume $\mathbf{r}_0 \equiv \mathbf{0}$.

We will expand $T \equiv \tau^2$ and $\{v_k\}_{k=0}^{\infty}$ as power series at **0**,

$$T = \sum_{\nu=0}^{\infty} T_{\nu}, \ v_k = \sum_{\nu=0}^{\infty} v_{k,\nu},$$

and assume the power series of **A**, N, β , and γ at **0** are already given as

$$\mathbf{A} = \sum_{\nu=0}^{\infty} \mathbf{A}_{\nu} \equiv \sum_{\nu=0}^{\infty} \begin{pmatrix} a_{\nu} & -c_{\nu} \\ -c_{\nu} & b_{\nu} \end{pmatrix}, \ N = \sum_{\nu=0}^{\infty} N_{\nu}, \ \beta = \sum_{\nu=0}^{\infty} \beta_{\nu}, \ \gamma = \sum_{\nu=0}^{\infty} \gamma_{\nu},$$

where $(\cdot)_{\nu}$ are homogeneous polynomials of degree ν in \mathbf{r} . We show how to determine $\{T_{\nu}\}$ and $\{v_{k,\nu}\}$ term by term for $\nu=0,1,2,\ldots$ For notational simplicity, we will denote $\Gamma_{\nu}\equiv(\beta_{\nu},\gamma_{\nu})$ for $\nu\geq0$, $D^2(\cdot)$ as the Hessian of a given function, and define

$$\begin{pmatrix} m_{11} & m_{12} \\ m_{21} & m_{22} \end{pmatrix} \odot \begin{pmatrix} n_{11} & n_{12} \\ n_{21} & n_{22} \end{pmatrix} \equiv m_{11}n_{11} + m_{12}n_{12} + m_{21}n_{21} + m_{22}n_{22}$$

for any two 2D tensors.

Power series expansion of T. From the anisotropic eikonal equation (8), we have $\nabla_{\mathbf{r}}T \cdot \mathbf{A} \cdot \nabla_{\mathbf{r}}T = 4NT$, which, with power series expansions, yields

$$\left(\sum_{\nu=1}^{\infty} \nabla_{\mathbf{r}} T_{\nu}\right) \cdot \left(\sum_{\nu=0}^{\infty} \mathbf{A}_{\nu}\right) \cdot \left(\sum_{\nu=1}^{\infty} \nabla_{\mathbf{r}} T_{\nu}\right) = 4 \left(\sum_{\nu=0}^{\infty} N_{\nu}\right) \left(\sum_{\nu=0}^{\infty} T_{\nu}\right).$$

By collecting terms of the same degree in \mathbf{r} , we can determine $\{T_{\nu}\}$ term by term.

 $T_0 = 0$ is obvious due to the initial condition $\tau(\mathbf{0}; \mathbf{0}) = 0$.

For \mathbf{r}^0 terms, we have $\nabla_{\mathbf{r}} T_1 \cdot \mathbf{A}_0 \cdot \nabla_{\mathbf{r}} T_1 = 0$, which implies $\nabla_{\mathbf{r}} T_1 = \mathbf{0}$, hence $T_1 = 0$. There are no \mathbf{r}^1 terms.

For \mathbf{r}^2 terms, we have $\nabla_{\mathbf{r}} T_2 \cdot \mathbf{A}_0 \cdot \nabla_{\mathbf{r}} T_2 = 4N_0T_2$, which implies $T_2 = N_0\mathbf{r} \cdot \mathbf{A}_0^{-1} \cdot \mathbf{r}$. This process can be repeated recursively. For $\nu \geq 3$, we have

$$2\nabla_{\mathbf{r}}T_{\nu}\cdot\mathbf{A}_{0}\cdot\nabla_{\mathbf{r}}T_{2}+\left(\sum_{l=2}^{\nu-1}\nabla_{\mathbf{r}}T_{l}\right)\cdot\left\{\sum_{s=2}^{\nu-l+1}\mathbf{A}_{\nu-l+2-s}\cdot\nabla_{\mathbf{r}}T_{s}\right\}=4N_{0}T_{\nu}+4\sum_{l=1}^{\nu-2}N_{l}T_{\nu-l},$$



which implies

$$T_{\nu} = \frac{4\sum_{l=1}^{\nu-2} N_{l} T_{\nu-l} - \left(\sum_{l=2}^{\nu-1} \nabla_{\mathbf{r}} T_{l}\right) \cdot \left\{\sum_{s=2}^{\nu-l+1} \mathbf{A}_{\nu-l+2-s} \cdot \nabla_{\mathbf{r}} T_{s}\right\}}{4(\nu-1)N_{0}},$$

where the right hand side only depends on T_p with p < v.

Therefore, we can determine $\{T_{\nu}\}$ term by term.

Power series expansion of $\{v_k\}$. By substituting the power series expansions into the transport equation (9) and collecting terms of the same degree in \mathbf{r} , we can derive the following formulas.

For \mathbf{r}^0 terms, we have

$$4(k-1)N_0v_{k,0} + (\mathbf{A}_0 \odot D_{\mathbf{r}}^2T_2)v_{k,0} = \Gamma_0 \cdot \nabla_{\mathbf{r}}v_{k-1,1} + \mathbf{A}_0 \odot D_{\mathbf{r}}^2v_{k-1,2},$$

which implies

$$v_{k,0} = \frac{\Gamma_0 \cdot \nabla_{\mathbf{r}} v_{k-1,1} + \mathbf{A}_0 \odot D_{\mathbf{r}}^2 v_{k-1,2}}{4k N_0}.$$

For \mathbf{r}^1 terms, we have

$$(\Gamma_{0} \cdot \nabla_{\mathbf{r}} T_{2}) v_{k,0} + 4(k-1) N_{0} v_{k,1} + 4(k-1) N_{1} v_{k,0}$$

$$+ (\mathbf{A}_{0} \odot D_{\mathbf{r}}^{2} T_{2}) v_{k,1} + [\mathbf{A}_{0} \odot D_{\mathbf{r}}^{2} T_{3} + \mathbf{A}_{1} \odot D_{\mathbf{r}}^{2} T_{2}] v_{k,0} + 2 \nabla_{\mathbf{r}} T_{2} \cdot \mathbf{A}_{0} \cdot \nabla_{\mathbf{r}} v_{k,1}$$

$$= \Gamma_{0} \cdot \nabla_{\mathbf{r}} v_{k-1,2} + \Gamma_{1} \cdot \nabla_{\mathbf{r}} v_{k-1,1} + \mathbf{A}_{0} \odot D_{\mathbf{r}}^{2} v_{k-1,3} + \mathbf{A}_{1} \odot D_{\mathbf{r}}^{2} v_{k-1,2},$$

which implies

$$v_{k,1} = \frac{\Gamma_0 \cdot \nabla_{\mathbf{r}} v_{k-1,2} + \Gamma_1 \cdot \nabla_{\mathbf{r}} v_{k-1,1} + \mathbf{A}_0 \odot D_{\mathbf{r}}^2 v_{k-1,3} + \mathbf{A}_1 \odot D_{\mathbf{r}}^2 v_{k-1,2}}{-(\Gamma_0 \cdot \nabla_{\mathbf{r}} T_2) v_{k,0} - 4(k-1) N_1 v_{k,0} - [\mathbf{A}_0 \odot D_{\mathbf{r}}^2 T_3 + \mathbf{A}_1 \odot D_{\mathbf{r}}^2 T_2] v_{k,0}}{4(k+1) N_0}.$$

This process can be repeated recursively. For $\nu \geq 2$, we have

$$\begin{split} &\sum_{l=0}^{\nu-1} \left\{ \sum_{s=0}^{\nu-l} (\Gamma_s \cdot \nabla_{\mathbf{r}} T_{\nu-l+1-s}) \right\} v_{k,l} + 4(k-1) N_0 v_{k,\nu} + 4(k-1) \sum_{l=0}^{\nu-1} N_{\nu-l} v_{k,l} \\ &+ (\mathbf{A}_0 \odot D_{\mathbf{r}}^2 T_2) v_{k,\nu} + \sum_{l=0}^{\nu-1} \left\{ \sum_{s=0}^{\nu-l} (\mathbf{A}_s \odot D_{\mathbf{r}}^2 T_{\nu-l-s+2}) \right\} v_{k,l} \\ &+ 2 \nabla_{\mathbf{r}} T_2 \cdot \mathbf{A}_0 \cdot v_{k,\nu} + 2 \sum_{l=0}^{\nu-1} \left\{ \sum_{s=0}^{\nu-l} \nabla_{\mathbf{r}} T_{s+1} \cdot \mathbf{A}_{\nu-l-s} \right\} \cdot v_{k,l} \\ &= \sum_{l=0}^{\nu} \Gamma_{\nu-l} \cdot \nabla_{\mathbf{r}} v_{k-1,l+1} + \sum_{l=0}^{\nu} \mathbf{A}_{\nu-l} \odot D_{\mathbf{r}}^2 v_{k-1,l+2}, \end{split}$$



which implies,

$$v_{k,\nu} = \frac{\sum_{l=0}^{\nu} \Gamma_{\nu-l} \cdot \nabla_{\mathbf{r}} v_{k-1,l+1} + \sum_{l=0}^{\nu} \mathbf{A}_{\nu-l} \odot D_{\mathbf{r}}^{2} v_{k-1,l+2} - \sum_{l=0}^{\nu-1} \left\{ \sum_{s=0}^{\nu-l} (\Gamma_{s} \cdot \nabla_{\mathbf{r}} T_{\nu-l+1-s}) \right\} v_{k,l} }{-4(k-1) \sum_{l=0}^{\nu-1} N_{\nu-l} v_{k,l} - \sum_{l=0}^{\nu-1} \left\{ \sum_{s=0}^{\nu-l} (\mathbf{A}_{s} \odot D_{\mathbf{r}}^{2} T_{\nu-l-s+2}) \right\} v_{k,l} }$$

$$v_{k,\nu} = \frac{-2 \sum_{l=0}^{\nu-1} \left\{ \sum_{s=0}^{\nu-l} \nabla_{\mathbf{r}} T_{s+1} \cdot \mathbf{A}_{\nu-l-s} \right\} \cdot v_{k,l}}{[4(k-1) + 4(\nu+1)] N_{0}}$$

where the right hand side only depends on $v_{k,p}$ with p < v and $v_{k-1,p}$ with $p \le v + 2$.

Therefore, we can determine $\{v_{k,\nu}\}$ term by term. The only term that can not be determined by the above formulas is $v_{0,0}$, which, however, can be determined by examining the solution of the anisotropic Helmholtz equation (1) with constant coefficients, i.e.,

$$\nabla_{\mathbf{r}} \cdot \mathbf{A}_0 \cdot \nabla_{\mathbf{r}} U + \omega^2 N_0 U = -\delta(\mathbf{r}). \tag{12}$$

Let $\mathbf{R} = \mathbf{A}_0^{-1/2} \cdot \mathbf{r}$, we have $\nabla_{\mathbf{r}} = \mathbf{A}_0^{-1/2} \cdot \nabla_{\mathbf{R}}$, which transforms Eq. (12) to the following isotropic case,

$$(\nabla_{\mathbf{R}} \cdot \nabla_{\mathbf{R}} + \omega^2 N_0) U(\mathbf{R}) = -\delta (\mathbf{A}_0^{1/2} \cdot \mathbf{R}) = -\frac{\delta(\mathbf{R})}{\sqrt{|\mathbf{A}_0|}}.$$
 (13)

The solution for Eq. (13) is given as

$$U(\mathbf{R}) = \begin{cases} \frac{1}{\sqrt{|\mathbf{A}_0|}} \frac{e^{\iota\omega\sqrt{N_0}|\mathbf{R}|}}{4\pi |\mathbf{R}|}, & 3D, \\ \frac{1}{\sqrt{|\mathbf{A}_0|}} \frac{\iota}{4} H_0^{(1)}(\omega\sqrt{N_0}|\mathbf{R}|), & 2D, \end{cases}$$

i.e.,

$$U(\mathbf{r}) = \begin{cases} \frac{1}{\sqrt{|\mathbf{A}_0|}} \frac{e^{i\omega\sqrt{N_0}\sqrt{\mathbf{r}\cdot\mathbf{A}_0^{-1}\cdot\mathbf{r}}}}{4\pi\sqrt{\mathbf{r}\cdot\mathbf{A}_0^{-1}\cdot\mathbf{r}}}, & 3D, \\ \frac{1}{\sqrt{|\mathbf{A}_0|}} \frac{\iota}{4} H_0^{(1)} \left(\omega\sqrt{N_0}\sqrt{\mathbf{r}\cdot\mathbf{A}_0^{-1}\cdot\mathbf{r}}\right), & 2D, \end{cases}$$

which, compared with the Babich's expansion (5), implies that

$$v_{0,0} = \begin{cases} \frac{1}{\sqrt{|\mathbf{A}_0|}} \frac{\sqrt{N_0}}{2\pi}, & 3D, \\ \frac{1}{\sqrt{|\mathbf{A}_0|}} \frac{1}{2\sqrt{\pi}}, & 2D. \end{cases}$$



Mesh	26×26	51 × 51	101×101	201 × 201
l_{∞} error for $ au$	1.026E-5	5.986E-7	1.808E-8	5.828E-10
order of conv.	_	4.099	5.049	4.955
l_{∞} error for v_0	4.576E-4	8.989E-5	9.460E-6	1.122E-6
order of conv.	_	2.348	3.248	3.076
l_{∞} error for v_1	3.879E-2	2.049E-2	7.218E-3	3.140E-3
order of conv.	_	0.921	1.505	1.201

Table 1 Order of convergence with l_{∞} errors for computing τ , v_0 and v_1

Reference solution is computed on a refined mesh (801×801) with the proposed methods

With the power series expansions, we can approximate τ and v_k up to any order P > 0 near the source, i.e., as $\mathbf{r} \to \mathbf{r}_0$,

$$\tau = \tau_P + O(|\mathbf{r} - \mathbf{r}_0|^P) \equiv \left(\sum_{\nu=2}^P T_\nu\right)^{1/2} + O(|\mathbf{r} - \mathbf{r}_0|^P),$$

$$v_k = \sum_{\nu=0}^{P-1} v_{k,\nu} + O(|\mathbf{r} - \mathbf{r}_0|^P).$$

For numerical implementation, we may choose $\tilde{\tau} = \tau_P$ near the source \mathbf{r}_0 , where P is the desired order of accuracy of the numerical scheme to be used.

Remark 1 For the current application, we can also apply the factorization approach with additive factors [8,19,20,22–24,26–29,31],

$$\tau = \tilde{\tau} + u$$

which leads to the following factored anisotropic eikonal equation for the smooth correction term u,

$$\sqrt{\nabla_{\mathbf{r}} u \cdot \mathbf{A} \cdot \nabla_{\mathbf{r}} u + 2\nabla_{\mathbf{r}} u \cdot \mathbf{A} \cdot \nabla_{\mathbf{r}} \tilde{\tau} + \nabla_{\mathbf{r}} \tilde{\tau} \cdot \mathbf{A} \cdot \nabla_{\mathbf{r}} \tilde{\tau}} = \frac{1}{v}.$$

This equation can also be used to compute high-order accurate phase τ with appropriate numerical schemes.

2.2.3 Lax-Friedrichs Schemes with WENO Approximations for Governing Equations

We apply the Lax–Friedrich scheme (LxF) [12,20,24,29,30,32] with weighted essentially non-oscillatory (WENO) finite-difference approximations [10,11,15,25] to numerically solve the factored anisotropic eikonal equation (11) and the transport equations (9). Without loss of generality, we present the methods in 2D spaces for the Hamilton-Jacobi type equation in a generic form as

$$H(x, z, u, u_x, u_z) = f(x, z),$$
 (14)

where H is the Hamiltonian that is convex in the gradient variables, and f is a given function. Assume the computational domain Ω is discretized by a uniform mesh $\{x_i, z_j\}$ for $i = 1, \ldots, I$, $j = 1, \ldots, J$ with the mesh size $\Delta x = (x_{\text{max}} - x_{\text{min}})/(I - 1)$, $\Delta z = (z_{\text{max}} - z_{\text{min}})/(J - 1)$. We also denote a grid point $(i, j) = (x_i, z_j)$ with neighbors $N\{i, j\} = (x_i, z_j)$



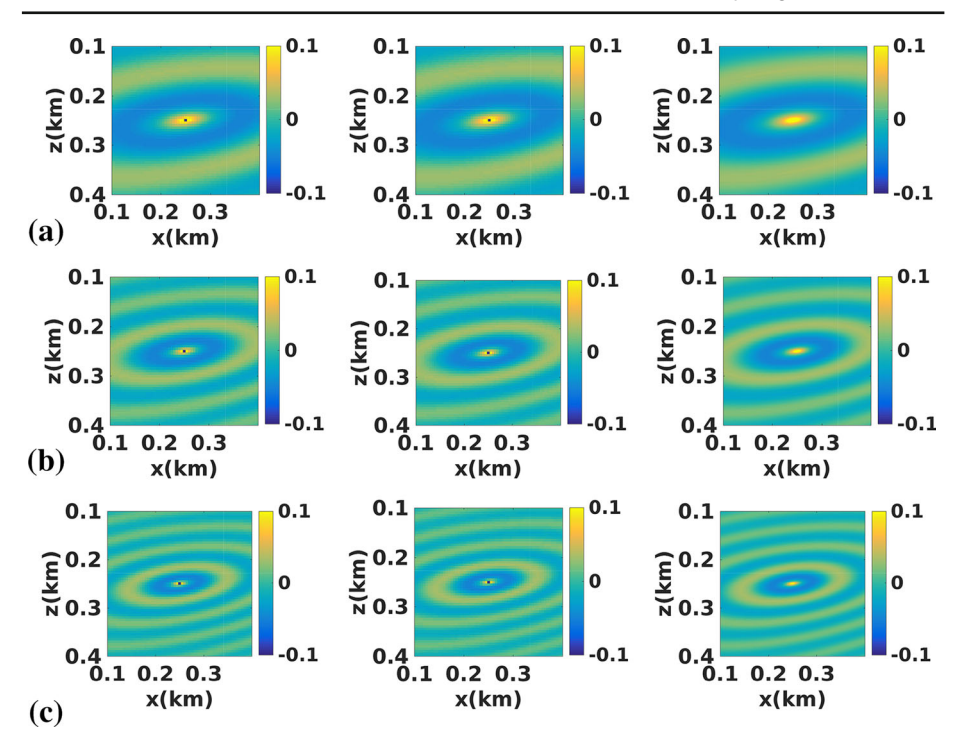


Fig. 1 Sinusoidal model, Case 1: real part of the wave with $\omega = 16\pi$ (a), 32π (b), and 48π (c). Left: U_1 , Middle: U_2 , Right: reference solution (Color figure online)

 $\{(x_{i-1}, z_j), (x_{i+1}, z_j), (x_i, z_{j-1}), (x_i, z_{j+1})\}$. We consider the following Lax–Friedrichs Hamiltonian [12,20,25],

$$H^{LF}(x_{i}, z_{j}, u_{i,j}, u_{N\{i,j\}}) = H\left(x_{i}, z_{j}, u_{i,j}, \frac{u_{i+1,j} - u_{i-1,j}}{2\Delta x}, \frac{u_{i,j+1} - u_{i,j-1}}{2\Delta z}\right) - \alpha_{x} \frac{u_{i+1,j} - 2u_{i,j} + u_{i-1,j}}{2\Delta x} - \alpha_{z} \frac{u_{i,j+1} - 2u_{i,j} + u_{i,j-1}}{2\Delta z},$$
(15)

where α_x and α_z are chosen such that at each grid point (x_i, z_j) ,

$$\frac{\partial H^{LF}}{\partial u_{i,j}} \ge 0, \ \frac{\partial H^{LF}}{\partial u_{N\{i,j\}}} \le 0. \tag{16}$$

Then we have the first-order Lax–Friedrichs scheme,

$$u_{i,j}^{new} = \left(\frac{1}{\alpha_x/\Delta x + \alpha_z/\Delta z}\right) \left[f_{i,j} - H\left(x_i, z_j, u_{i,j}^{old}, \frac{u_{i+1,j} - u_{i-1,j}}{2\Delta x}, \frac{u_{i,j+1} - u_{i,j-1}}{2\Delta z}\right) + \alpha_x \frac{u_{i+1,j} + u_{i-1,j}}{2\Delta x} + \alpha_z \frac{u_{i,j+1} + u_{i,j-1}}{2\Delta z}\right].$$
(17)

As in [20,23,32], we can replace $u_{i-1,j}$, $u_{i+1,j}$, $u_{i,j-1}$ and $u_{i,j+1}$ as,

$$u_{i-1,j} = u_{i,j} - \Delta x(u_x)_{i,j}^-, \ u_{i+1,j} = u_{i,j} + \Delta x(u_x)_{i,j}^+; u_{i,j-1} = u_{i,j} - \Delta z(u_x)_{i,j}^-, \ u_{i,j+1} = u_{i,j} + \Delta z(u_x)_{i,j}^+.$$
(18)



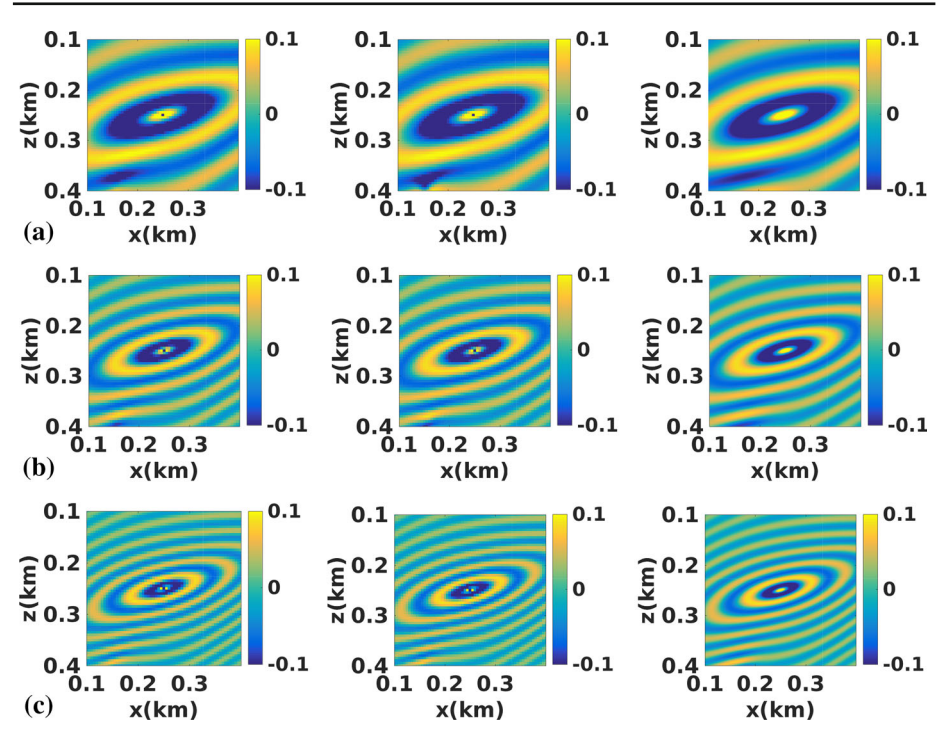


Fig. 2 Sinusoidal model, Case 2: real part of the wave with $\omega = 16\pi$ (a), 32π (b), and 48π (c). Left: U_1 , Middle: U_2 , Right: reference solution (Color figure online)

Here, $(u_x)_{i,j}^-$ and $(u_x)_{i,j}^+$ are high-order WENO approximations of u_x , and $(u_z)_{i,j}^-$ and $(u_z)_{i,j}^+$ are high-order WENO approximations of u_z ; see [10,11,15,25]. Then we have the following high-order Lax–Friedrichs scheme based on high-order WENO approximations [20,32],

$$u_{i,j}^{new} = \left(\frac{1}{\alpha_x/\Delta x + \alpha_z/\Delta z}\right) \left[f_{i,j} - H\left(x_i, z_j, u_{i,j}^{old}, \frac{(u_x)_{i,j}^- + (u_x)_{i,j}^+}{2}, \frac{(u_x)_{i,j}^- + (u_x)_{i,j}^+}{2}\right) + \alpha_x \frac{2u_{i,j}^{old} + \Delta x[(u_x)_{i,j}^+ - (u_x)_{i,j}^-]}{2\Delta x} + \alpha_z \frac{2u_{i,j}^{old} + \Delta z[(u_x)_{i,j}^+ - (u_x)_{i,j}^-]}{2\Delta z}\right].$$
(19)

In the updating formulas (17) and (19), $u_{i,j}^{new}$ and $u_{i,j}^{old}$ denote the to-be-updated numerical solution and the current old value for u at the grid point (x_i, z_j) , respectively.

The algorithm is summarized here.

Algorithm 1 (LxF Scheme with WENO approximations for Eq. (14))

1. Initialization:

For grid points in a $\Delta x \times \Delta z$ (first-order), $2\Delta x \times 2\Delta z$ (WENO3), or $3\Delta x \times 3\Delta z$ (WENO5) small neighborhood covering the source, their values are set and fixed according to the boundary conditions. All other points are assigned a large value initially.



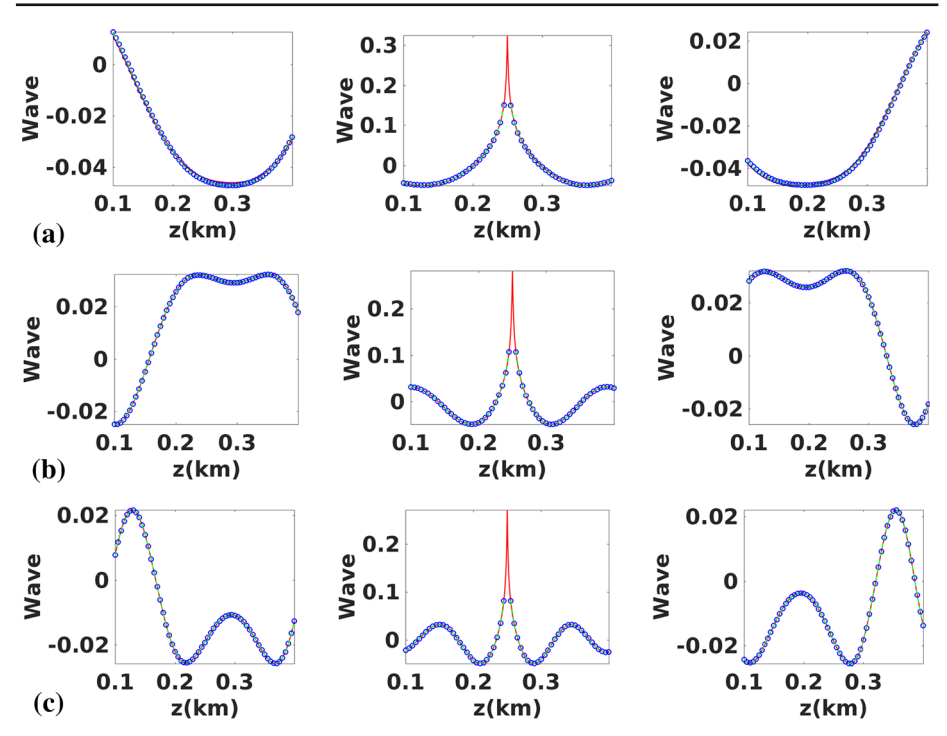


Fig. 3 Sinusoidal model, Case 1: real part of the wave with $\omega = 16\pi$ (a), 32π (b), and 48π (c). Blue-circle: U_1 , Green-dash: U_2 , and Red-line: reference solution. Left: at z=0.2 (km), Middle: at z=0.25 (km), and Right: at z=0.3 (km) (Color figure online)

2. Gauss-Seidel iterations with alternating orderings (sweepings):

- Sweepings: sweep all the grid points following the four alternating orderings,

(1)
$$i = 1:I$$
; $j = 1:J$; (2) $i = I:1$; $j = 1:J$;
(3) $i = I:1$; $j = J:1$; (4) $i = 1:I$; $j = J:1$.

- Updating: at each point (x_i, z_j) , the updated value $u_{i,j}^{new}$ is computed from the current given neighboring values according to the procedure detailed above.
- Stopping criterion: given $\delta > 0$, check if $|u^{new} u^{old}| < \delta$.

2.2.4 Implementation Details

The infinite series in the Babich's expansion (5) needs to be truncated to approximate the wave U for practical applications. In this work, we will approximate U as

$$U \approx U_1 \equiv v_0 f_0$$
, or $U \approx U_2 \equiv v_0 f_0 + v_1 f_1$.

With the scheme presented in Algorithm 1, we will use the LxF scheme with WENO5 approximations (LxF-WENO5) to solve the factored anisotropic eikonal equation (11) for τ , where the values at points near the source are initialized using the fifth-order power-series approximation, and we will use the LxF scheme with WENO3 approximations (LxF-WENO3) and first-order approximations (LxF-1st) to solve the transport equation (9) for v_0 and v_1 , respectively, where the values at points near the source are initialized using the third-order power-series approximations.



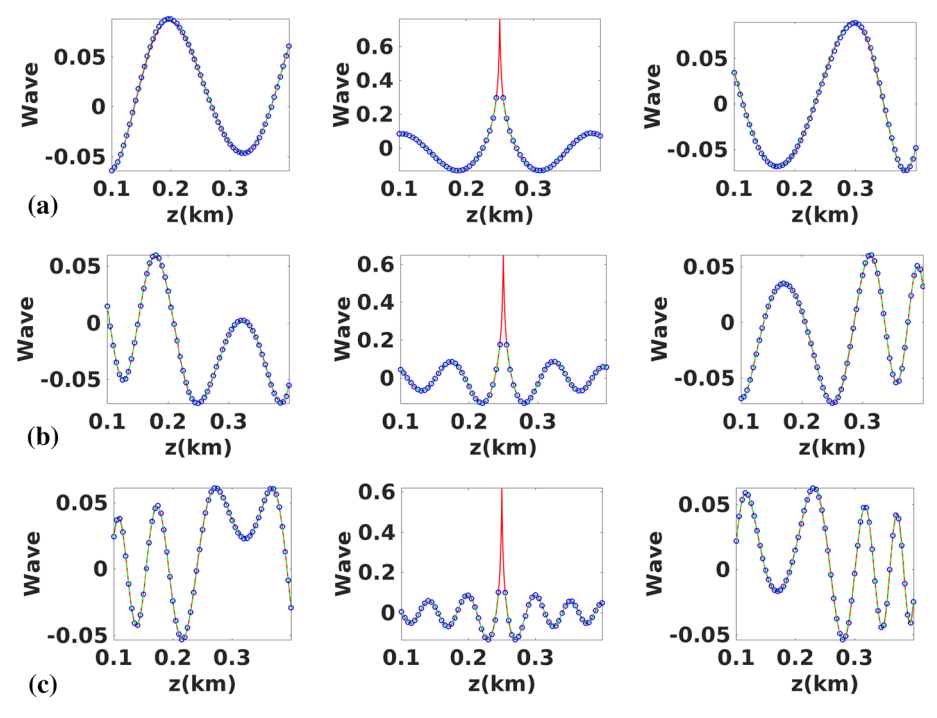


Fig. 4 Sinusoidal model, Case 2: real part of the wave with $\omega=16\pi$ (a), 32π (b), and 48π (c). Blue-circle: U_1 , Green-dash: U_2 , and Red-line: reference solution. Left: at z=0.2 (km), Middle: at z=0.25 (km), and Right: at z=0.3 (km) (Color figure online)

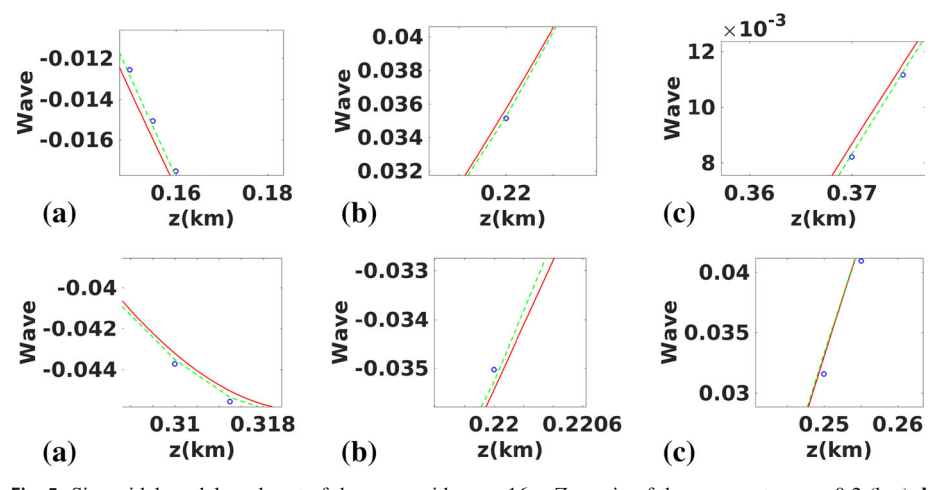


Fig. 5 Sinusoidal model: real part of the wave with $\omega = 16\pi$. Zoom-in of the curves at $\mathbf{a} z = 0.2$ (km), $\mathbf{b} z = 0.2$ (km), and $\mathbf{c} : z = 0.3$ (km). Top: Case 1; Bottom: Sase 2. Blue-circle: U_1 , Green-dash: U_2 , and Red-line: reference solution (Color figure online)



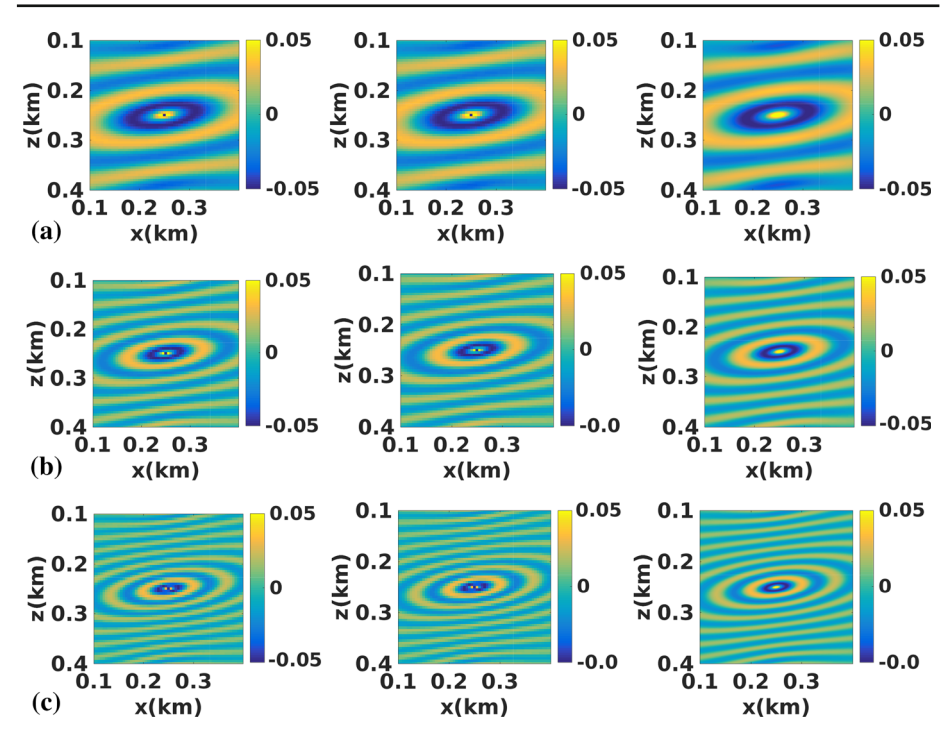


Fig. 6 Waveguide model, Case 1: real part of the wave with $\omega = 16\pi$ (a), 32π (b), and 48π (c). Left: U_1 , Middle: U_2 , and Right: reference solution (Color figure online)

The WENO3 approximations, for example for $(u_x)_{i,j}^-$ and $(u_x)_{i,j}^+$, are given as

$$(u_x)_{i,j}^- = \frac{1}{2} \left(\frac{\Delta^+ u_{i-1,j}}{\Delta x} + \frac{\Delta^+ u_{i,j}}{\Delta x} \right) - \frac{w_-}{2} \left(\frac{\Delta^+ u_{i-2,j}}{\Delta x} - 2 \frac{\Delta^+ u_{i-1,j}}{\Delta x} + \frac{\Delta^+ u_{i,j}}{\Delta x} \right),$$

with

$$w_{-} = \frac{1}{1 + 2r^2}, \ r = \frac{\epsilon + (\Delta^{-} \Delta^{+} u_{i-1,j})^2}{\epsilon + (\Delta^{-} \Delta^{+} u_{i,j})^2},$$

and

$$(u_x)_{i,j}^+ = \frac{1}{2} \left(\frac{\Delta^+ u_{i-1,j}}{\Delta x} + \frac{\Delta^+ u_{i,j}}{\Delta x} \right) + \frac{w_+}{2} \left(\frac{\Delta^+ u_{i+1,j}}{\Delta x} - 2 \frac{\Delta^+ u_{i,j}}{\Delta x} + \frac{\Delta^+ u_{i-1,j}}{\Delta x} \right),$$

with

$$w_{+} = \frac{1}{1 + 2r^{2}}, \ r = \frac{\epsilon + (\Delta^{-} \Delta^{+} u_{i+1,j})^{2}}{\epsilon + (\Delta^{-} \Delta^{+} u_{i,j})^{2}}.$$

The WENO5 approximations, for example for $(u_x)_{i,j}^-$ and $(u_x)_{i,j}^+$, are given as

$$\begin{split} (u_x)_{i,j}^- &= \frac{1}{12} \left(-\frac{\Delta^+ u_{i-2,j}}{\Delta x} + 7\frac{\Delta^+ u_{i-1,j}}{\Delta x} + 7\frac{\Delta^+ u_{i,j}}{\Delta x} - \frac{\Delta^+ u_{i+1,j}}{\Delta x} \right) \\ &- \Phi^{WENO} \left(\frac{\Delta^- \Delta^+ u_{i-2,j}}{\Delta x}, \frac{\Delta^- \Delta^+ u_{i-1,j}}{\Delta x}, \frac{\Delta^- \Delta^+ u_{i,j}}{\Delta x}, \frac{\Delta^- \Delta^+ u_{i+1,j}}{\Delta x} \right), \end{split}$$



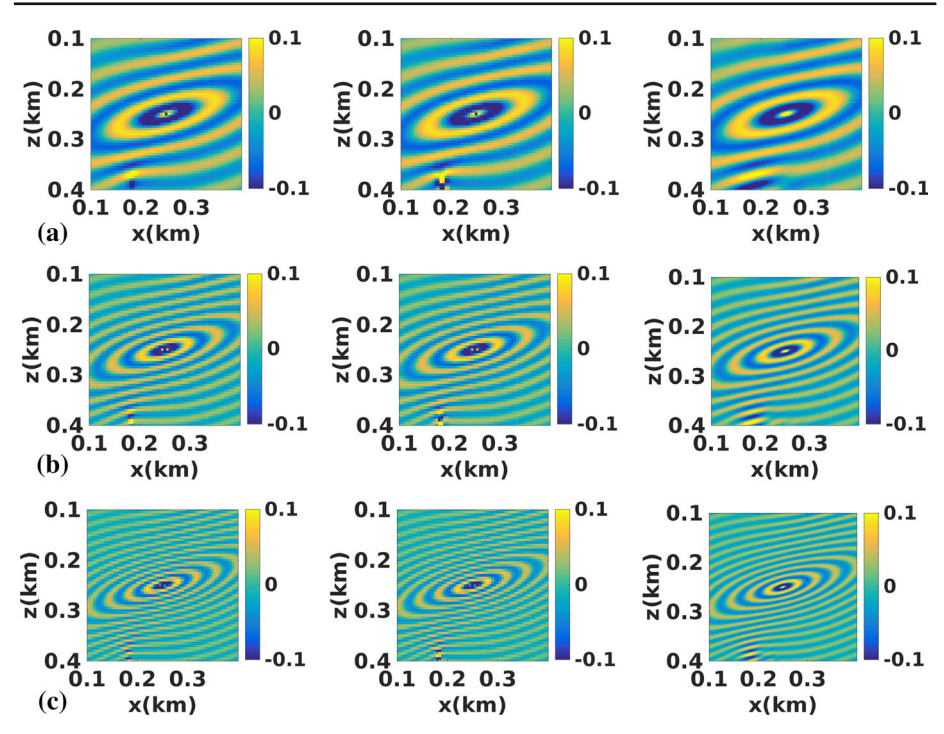


Fig. 7 Waveguide model, Case 2: real part of the wave with $\omega=16\pi$ (a), 32π (b), and 48π (c). Left: U_1 , Middle: U_2 , and Right: reference solution (Color figure online)

with

$$\Phi^{WENO}(a, b, c, d) = \frac{1}{3}w_0(a - 2b + c) + \frac{1}{6}\left(w_2 - \frac{1}{2}\right)(b - 2c + d),$$

$$w_0 = \frac{\alpha_0}{\alpha_0 + \alpha_1 + \alpha_2}, \quad w_2 = \frac{\alpha_2}{\alpha_0 + \alpha_1 + \alpha_2},$$

$$\alpha_0 = \frac{1}{(\epsilon + IS_0)^2}, \quad \alpha_1 = \frac{6}{(\epsilon + IS_1)^2}, \quad \alpha_2 = \frac{3}{(\epsilon + IS_2)^2},$$

$$IS_0 = 13(a - b)^2 + 3(a - 3b)^2, \quad IS_1 = 13(b - c)^2 + 3(b + c)^2,$$

$$IS_1 = 13(c - d)^2 + 3(3c - d)^2.$$

and

$$(u_{x})_{i,j}^{+} = \frac{1}{12} \left(-\frac{\Delta^{+}u_{i-2,j}}{\Delta x} + 7\frac{\Delta^{+}u_{i-1,j}}{\Delta x} + 7\frac{\Delta^{+}u_{i,j}}{\Delta x} - \frac{\Delta^{+}u_{i+1,j}}{\Delta x} \right) - \Phi^{WENO} \left(\frac{\Delta^{-}\Delta^{+}u_{i+2,j}}{\Delta x}, \frac{\Delta^{-}\Delta^{+}u_{i+1,j}}{\Delta x}, \frac{\Delta^{-}\Delta^{+}u_{i,j}}{\Delta x}, \frac{\Delta^{-}\Delta^{+}u_{i-1,j}}{\Delta x} \right).$$

The parameter ϵ is chosen as 10^{-6} to avoid division by zero, and $\Delta^{\pm}u_{i,j} \equiv \pm (u_{i\pm 1,j} - u_{i,j})$. For computing phase τ , we choose $\tilde{\tau} = \tau_P$ with P = 5 to achieve the desired fifth-order accuracy. Since τ_P is in general well-defined in a neighborhood of the primary source \mathbf{r}_0 , we can use the Hybrid scheme [23], where the factored equation (11) is solved in a neighborhood



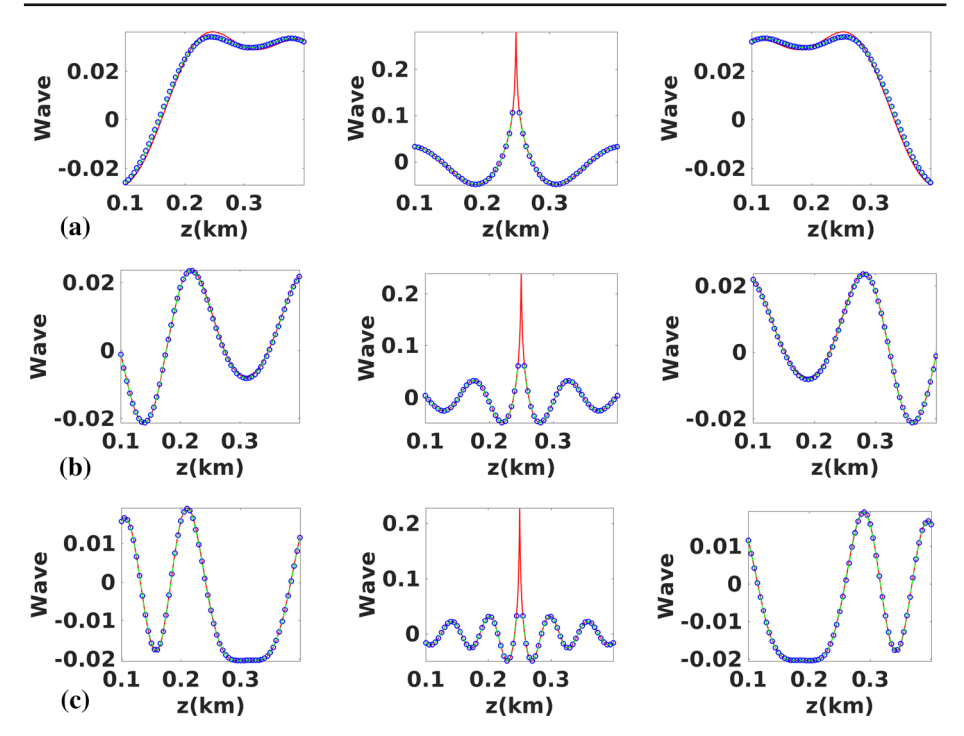


Fig. 8 Waveguide model, Case 1: real part of the wave with $\omega=16\pi$ (a), 32π (b), and 48π (c). Blue-circle: U_1 , Green-dash: U_2 , and Red-line: reference solution. Left: at z=0.2 (km), Middle: at z=0.25 (km), and Right: at z=0.3 (km) (Color figure online)

of the primary source \mathbf{r}_0 and the original Eq. (8) is solved outside this neighborhood. The size of this neighborhood is independent of the mesh and can be determined easily.

When applying the LxF-WENO schemes for solving the governing equations, we will impose the computational boundary conditions introduced in [12] to enforce outgoing boundary conditions. Therefore, the solutions will reduce to first-order accurate near the computational boundary. However, the computational boundary conditions will not affect the high-order accuracy of the solutions in the interior of the computational domain. Once τ , v_0 and v_1 are computed, we can use them repeatedly to construct waves as U_1 or U_2 for any high frequencies.

3 Numerical Examples

In this section, we present numerical examples to demonstrate the methods. Reference solutions are obtained by the finite difference methods with central differences on very refined meshes.

Example 1: Sinusoidal Velocity Model. We consider the following parameters:

- The velocity $v(x, z) = 1 + 0.2 \sin(3\pi(x + 0.05)) \sin(0.5\pi z) \text{(km/s)}.$
- The computational domain is $\Omega = [0, 0.5]^2$ (km), and the source is $\mathbf{r}_0 = (0.25, 0.25)$ (km).



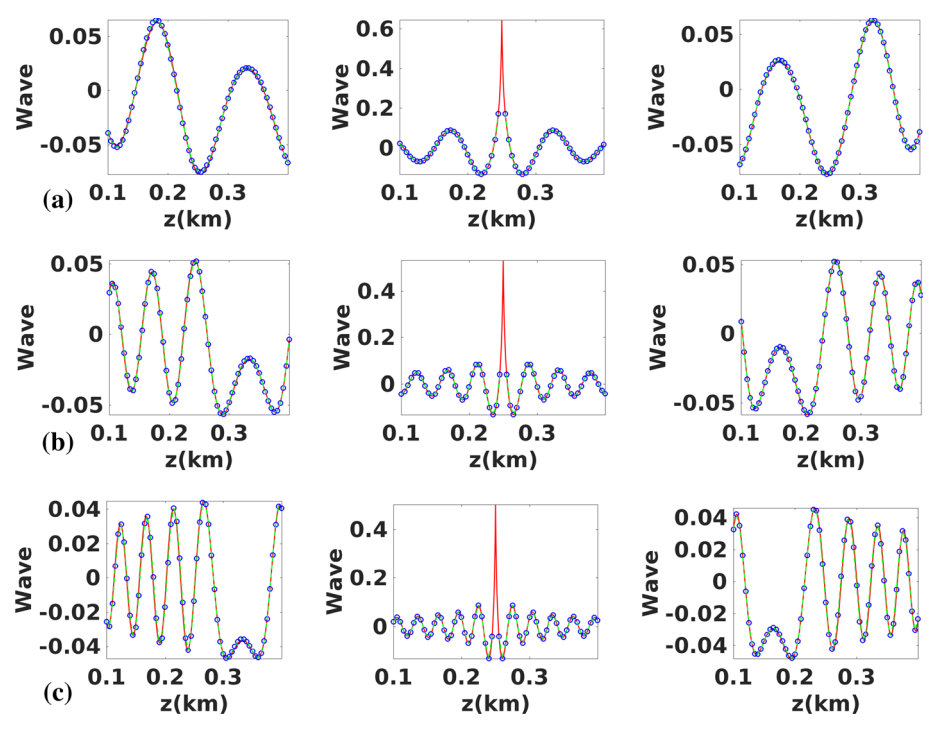


Fig. 9 Waveguide model, Case 2: real part of the wave with $\omega = 16\pi$ (a), 32π (b), and 48π (c). Blue-circle: U_1 , Green-dash: U_2 , and Red-line: reference solution. Left: at z=0.2 (km), Middle: at z=0.25 (km), and Right: at z=0.3 (km) (Color figure online)

The anisotropy tensor A is chosen as

$$\mathbf{A} = \begin{pmatrix} 8 & -1 \\ -1 & 1 \end{pmatrix} \text{ (Case 1)}, \text{ or}$$

$$\mathbf{A} = \begin{pmatrix} 1.5025(1 + \sin^2(8\pi xz)) & -0.8616953(1 - 0.125\sin^2(8\pi xz)) \\ -0.8616953(1 - 0.125\sin^2(8\pi xz)) & 0.5075(1 + \cos^2(8\pi xz)) \end{pmatrix} \text{ (Case 2)}.$$

- The mesh for computing the phase and amplitude terms is 101×101 .
- The mesh for computing the reference solution is 801×801 for $\omega = 16\pi, 32\pi$, and 1001×1001 for $\omega = 48\pi$.

Table 1 shows the l_{∞} errors for computing τ , v_0 and v_1 with the proposed approaches. We observe the desired fifth, third and first order of convergence for τ , v_0 and v_1 , respectively.

Figures 1 and 2 show plots of the numerical solutions and reference solutions. Figures 3 and 4 show detailed comparisons between the numerical solutions and the reference solutions. And Fig. 5 shows zoom-in portion of the figures.

Example 2: Waveguide Velocity Model. We consider the following parameters:

- The velocity $v(x, z) = 1 0.5e^{-16(x 0.25)^2}$ (km/s).
- The computational domain is $\Omega = [0, 0.5]^2$ (km), and the source is $\mathbf{r}_0 = (0.25, 0.25)$ (km).



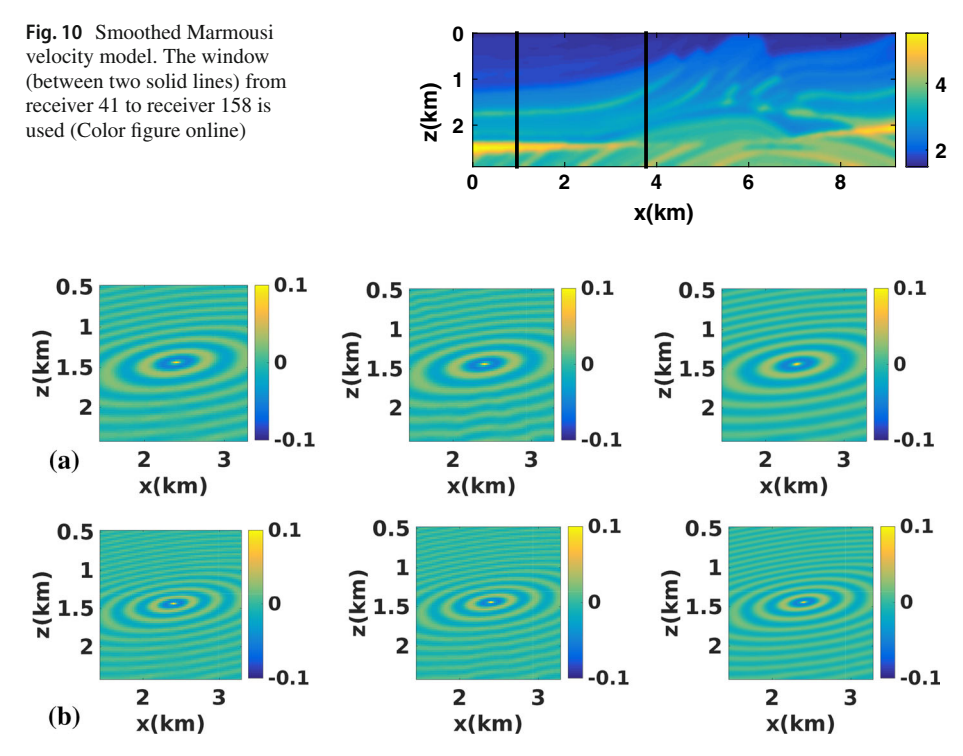


Fig. 11 Marmousi model, Case 1: real part of the wave with $\omega = 32\pi$ (a), and 48π (b). Left: U_1 , Middle: U_2 , Right: reference solution (Color figure online)

The anisotropy tensor A is chosen as

$$\mathbf{A} = \begin{pmatrix} 8 & -1 \\ -1 & 1 \end{pmatrix} \text{ (Case 1), or}$$

$$\mathbf{A} = \begin{pmatrix} 1.5025(1 + \sin^2(8\pi xz)) & -0.8616953(1 - 0.125\sin^2(8\pi xz)) \\ -0.8616953(1 - 0.125\sin^2(8\pi xz)) & 0.5075(1 + \cos^2(8\pi xz)) \end{pmatrix} \text{ (Case 2)}.$$

- The mesh for computing the phase and amplitude terms is 101×101 .
- The mesh for computing the reference solution is 801×801 for $\omega = 16\pi, 32\pi$, and 1001×1001 for $\omega = 48\pi$.

Figures 6 and 7 show plots of the numerical solutions and reference solutions. Figures 8 and 9 show detailed comparisons between the numerical solutions and the reference solutions.

Example 3: Marmousi Velocity Model. We consider the following parameters:

- The velocity v(x, z) is chosen to be a window (receiver 41 to 158) of the Marmousi model, referring to Fig. 10.
- The computational domain is $\Omega = [0.96, 3.768] \times [0, 2.094]$ (km), and the source is $\mathbf{r}_0 = (2.4, 1.44)$ (km).



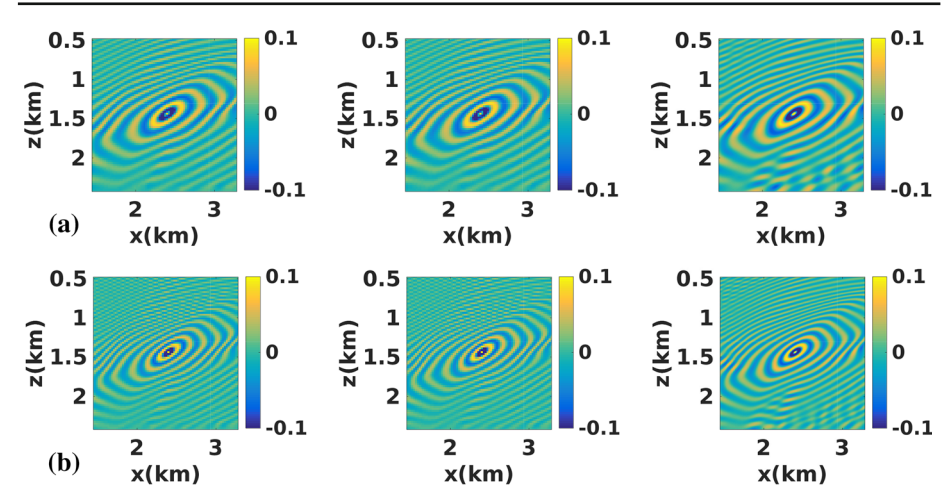


Fig. 12 Marmousi model, Case 2: real part of the wave with $\omega = 32\pi$ (a), and 48π (b). Left: U_1 , Middle: U_2 , Right: reference solution (Color figure online)

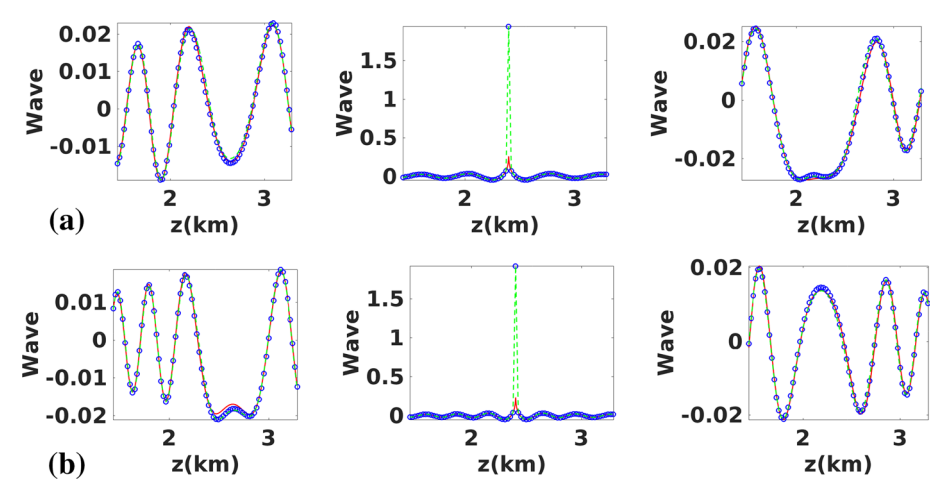


Fig. 13 Marmousi model, Case 1: real part of the wave with $\omega = 32\pi$ (a), 48π (b). Blue-circle: U_1 , Greendash: U_2 , and Red-line: reference solution. Left: at z=2.16 (km), Middle: at z=2.4 (km), and Right: z=2.64 (km) (Color figure online)

- The anisotropy tensor **A** is chosen as

$$\mathbf{A} = \begin{pmatrix} 8 & -1 \\ -1 & 1 \end{pmatrix} \text{ (Case 1), or}$$

$$\mathbf{A} = \begin{pmatrix} 1.5025(1 + \sin^2(\pi xz)) & -0.8616953(1 - 0.125\sin^2(\pi xz)) \\ -0.8616953(1 - 0.125\sin^2(\pi xz)) & 0.5075(1 + \cos^2(\pi xz)) \end{pmatrix} \text{ (Case 2)}.$$

- The mesh for computing the phase and amplitude terms is 118×122 .
- The mesh for computing the reference solution is 1171×1211 .
- For computing the reference solutions, the velocity is interpolated onto a refined mesh by cubic polynomials.



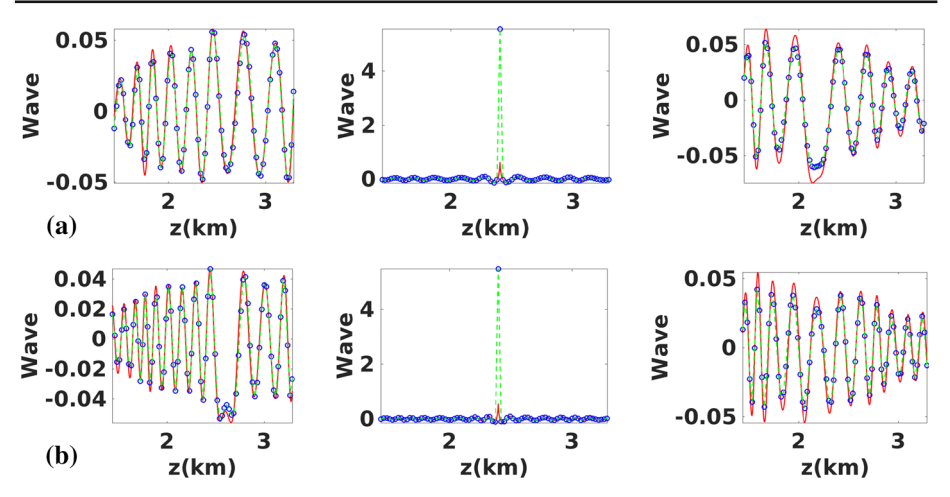


Fig. 14 Marmousi model, Case 2: real part of the wave with $\omega=32\pi$ (a), 48π (b). Blue-circle: U_1 , Greendash: U_2 , and Red-line: reference solution. Left: at z=2.16 (km), Middle: at z=2.4 (km), and Right: z=2.64 (km) (Color figure online)

Figures 11 and 12 show plots of the numerical solutions and reference solutions. Figures 13 and 14 show detailed comparisons between the numerical solutions and the reference solutions.

3.1 Discussion of Numerical Examples

For all the examples, the phase and amplitude terms are computed on a coarse mesh, and are re-used to construct the waves for different frequencies.

If there are no caustics, the computed numerical solutions approximate the reference solutions faithfully, which verifies the feasibility of the proposed methods. In particular, uniform accuracy near the source is achieved, see second columns of Figs. 3, 4, 8, 9, 13, and 14.

If the caustics occur, the proposed methods can not capture caustics faithfully, which is common for high frequency asymptotic approaches. In future work, we will incorporate the proposed methods to the fast Huygens sweeping method [22,27–29] such that the caustics can be captured faithfully.

4 Conclusion

We present asymptotic approaches for solving high frequency anisotropic Helmholtz equation with a point-source condition. The methods are based on Babich's expansion that was first introduced for isotropic Helmholtz equation. Detailed formulations for the governing equations of the phase and amplitude terms are derived, and efficient high-order schemes, with high-order approximations near the source, are designed to solve the governing equations. The solutions can be used to reconstruct the waves for different high frequencies. Numerical experiments verify the effectiveness of the methods.

The proposed methods can be incorporated into the fast Huygens sweeping method [22, 27–29] for capturing the caustics faithfully for the anisotropic Helmholtz equation, where



the proposed method will provide numerical approximations for Green's functions that are needed in the fast Huygens sweeping method. The results will be reported in future work.

Acknowledgements Funding was provided by NSF Division of Mathematical Sciences (1418908, 1719907).

Appendix A: WKB Approximation for Eq. (1) in 2D

We derive the governing equations for the phase and amplitude terms in the WKB expansion (2) for the anisotropic Helmholtz equation (1) in 2D.

Theorem 2 In the WKB approximation (2) for the anisotropic Helmholtz equation (1) in 2D, the phase τ satisfies the anisotropic eikonal equation (8), and the amplitude terms $\{A_k\}_{k=0}^{\infty}$ satisfy the following recurrent system,

$$\begin{split} A_{-1} &\equiv 0, \\ &(\beta \tau_x + \gamma \tau_z + a \tau_{xx} - 2c\tau_{xz} + b\tau_{zz})A_k + 2\{(a\tau_x - c\tau_z)(A_k)_x + (b\tau_z - c\tau_x)(A_k)_\xi (21)\} \\ &= -(\beta (A_{k-1})_x + \gamma (A_{k-1})_z) - (a(A_{k-1})_{xx} - 2c(A_{k-1})_{xz} + b(A_{k-1})_{zz}), \ k \geq 0, \end{split}$$
 where $\beta \equiv a_x - c_z$, and $\gamma \equiv b_z - c_x$.

Theorem 2 can be proved by careful calculation. We have

$$\begin{split} U_x &= \sum_{k=0}^{\infty} \left(\frac{\tau_x A_k}{(\iota \omega)^{k-1}} + \frac{(A_k)_x}{(\iota \omega)^k} \right) e^{\iota \omega \tau}; \\ U_z &= \sum_{k=0}^{\infty} \left(\frac{\tau_z A_k}{(\iota \omega)^{k-1}} + \frac{(A_k)_z}{(\iota \omega)^k} \right) e^{\iota \omega \tau}; \\ U_{xx} &= \sum_{k=0}^{\infty} \left(\frac{\tau_x^2 A_k}{(\iota \omega)^{k-2}} + \frac{2\tau_x (A_k)_x + \tau_{xx} A_k}{(\iota \omega)^{k-1}} + \frac{(A_k)_{xx}}{(\iota \omega)^k} \right) e^{\iota \omega \tau}; \\ U_{zz} &= \sum_{k=0}^{\infty} \left(\frac{\tau_z^2 A_k}{(\iota \omega)^{k-2}} + \frac{2\tau_z (A_k)_z + \tau_{zz} A_k}{(\iota \omega)^{k-1}} + \frac{(A_k)_{zz}}{(\iota \omega)^k} \right) e^{\iota \omega \tau}; \\ U_{xz} &= U_{xz} &= \sum_{k=0}^{\infty} \left(\frac{\tau_x \tau_z A_k}{(\iota \omega)^{k-2}} + \frac{\tau_z (A_k)_x + \tau_x (A_k)_z + \tau_{xz} A_k}{(\iota \omega)^{k-1}} + \frac{(A_k)_{xz}}{(\iota \omega)^k} \right) e^{\iota \omega \tau}. \end{split}$$

By substitution the above formulas into Eq. (1), we have

$$\begin{split} &\sum_{k=0}^{\infty} \left(\frac{A_k}{(\iota \omega)^{k-2}} \{ a \tau_x^2 - 2 c \tau_x \tau_z + b \tau_z^2 - 1/v^2 \} \right. \\ &+ \frac{1}{(\iota \omega)^{k-1}} \{ (\beta \tau_x + \gamma \tau_z + a \tau_{xx} - 2 c \tau_{xz} + b \tau_{zz}) A_k \\ &+ 2 (a \tau_x - c \tau_z) (A_k)_x + 2 (b \tau_z - c \tau_x) (A_k)_z \} \\ &+ \frac{1}{(\iota \omega)^k} \{ \beta (A_k)_x + \gamma (A_k)_z + a (A_k)_{xx} - 2 c (A_k)_{xz} + b (A_k)_{zz} \} \right) e^{\iota \omega \tau} = 0. \end{split}$$

Then collecting coefficient for $O(1/(\iota\omega)^{k-2})$ term and letting it be equal to 0 yields the anisotropic eikonal equation (8), and collecting coefficients for $O(1/(\iota\omega)^{k-1})$ term and let it be equal to 0 yields the recurrent system (21).



The factorization techniques can also be applied to resolve the source singularities for computing amplitude terms $\{A_k\}_{k=0}^{\infty}$, for instance, see [22,24,28] for similar techniques applied for isotropic cases.

Appendix B: WKB Approximation and Babich's Expansion for Eq. (1) in 3D

We also include the formulations of the WKB approximation and Babich's expansion for the anisotropic Helmholtz equation (1) in three-dimensional (3D) spaces. We assume the anisotropy tensor **A** is given as

$$\mathbf{A}(\mathbf{r}) = \begin{pmatrix} a(\mathbf{r}) & -d(\mathbf{r}) & -e(\mathbf{r}) \\ -d(\mathbf{r}) & b(\mathbf{r}) & -f(\mathbf{r}) \\ -e(\mathbf{r}) & -f(\mathbf{r}) & c(\mathbf{r}) \end{pmatrix}.$$

Theorem 3 In the WKB approximation (2) for the anisotropic Helmholtz equation (1) in 3D, the phase τ satisfies the anisotropic eikonal equation (8), and the amplitude terms $\{A_k\}_{k=0}^{\infty}$ satisfy the following recurrent system,

$$A_{-1} \equiv 0,$$

$$(\beta \tau_{x} + \gamma \tau_{y} + \zeta \tau_{z} + a \tau_{xx} + b \tau_{yy} + c \tau_{zz} - 2d \tau_{xy} - 2e \tau_{xz} - 2f \tau_{yz}) A_{k}$$

$$+ 2\{(a \tau_{x} - d \tau_{y} - e \tau_{z})(A_{k})_{x}$$

$$+ (b \tau_{y} - d \tau_{x} - f \tau_{z})(A_{k})_{y} + (c \tau_{z} - e \tau_{x} - f \tau_{y})(A_{k})_{z}\}$$

$$= -(\beta (A_{k-1})_{x} + \gamma (A_{k-1})_{y} + \zeta (A_{k-1})_{z})$$

$$- (a(A_{k-1})_{xx} + b(A_{k-1})_{yy} + c(A_{k-1})_{zz}$$

$$- 2d(A_{k-1})_{xy} - 2e(A_{k-1})_{xz} - 2f(A_{k-1})_{yz}), k \geq 0,$$

$$where \beta \equiv a_{x} - d_{y} - e_{z}, \gamma \equiv b_{y} - d_{x} - f_{z}, and \zeta = c_{z} - e_{x} - f_{y}.$$

$$(22)$$

Theorem 4 In the Babich's expansion (5) for the anisotropic Helmholtz equation (1) in 3D, the phase τ satisfies the anisotropic eikonal equation (8), and the amplitude terms $\{v_k\}_{k=0}^{\infty}$ satisfy the following recurrent system,

$$v_{-1} \equiv 0,$$

$$(\beta T_x + \gamma T_y + \zeta T_z + (4k - 6)N + aT_{xx} + bT_{yy} + cT_{zz} - 2dT_{xy} - 2eT_{xz} - 2fT_{yz})v_k$$

$$+ 2\{(aT_x - dT_y - eT_z)(v_k)_x + (bT_y - dT_x - fT_z)(v_k)_y$$

$$+ (cT_z - eT_x - fT_y)(v_k)_z\}$$

$$= (\beta(v_{k-1})_x + \gamma(v_{k-1})_y + \zeta(v_{k-1})_z)$$

$$+ (a(v_{k-1})_{xx} + b(v_{k-1})_{yy} + c(v_{k-1})_{zz}$$

$$- 2d(v_{k-1})_{xy} - 2e(v_{k-1})_{xz} - 2f(v_{k-1})_{yz}), \ k \ge 0,$$

$$where \ \beta \equiv a_x - d_y - e_z, \ \gamma \equiv b_y - d_x - f_z, \ \zeta = c_z - e_x - f_y, \ N \equiv 1/v^2, \ and \ T \equiv \tau^2.$$

Theorems 3 and 4 can be proved similarly as in 2D cases. And the governing equations for τ and $\{v_k\}$ can be solved by the same schemes numerically. Figures 15 and 16 show plots of a 3D model on computational domain $[0, 0.5]^3$ (km) with

$$v(\mathbf{r}) = 3 - 1.75e^{-((x-0.25)^2 + (y-0.25)^2 + (z-0.25)^2)/0.64} (\text{km/s}).$$



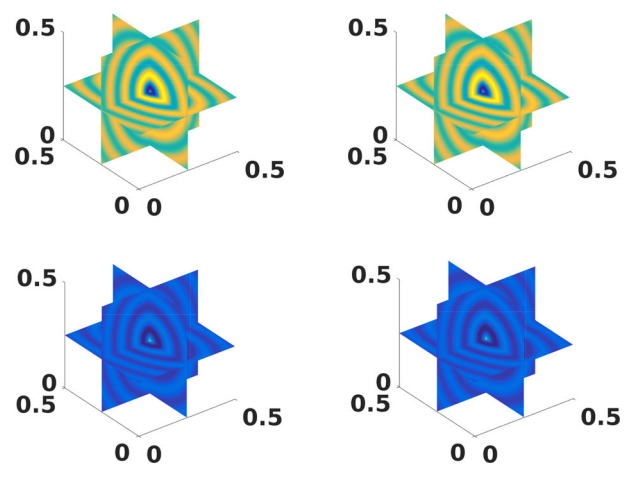


Fig. 15 3D model. Case 1: slices of the wave with $\omega = 32\pi$ at x = 0.25 (km), y = 0.25 (km) and z = 0.25 (km), respectively. Top: real part; Bottom: imaginary part. Left: U_1 ; Right: U_2 (Color figure online)

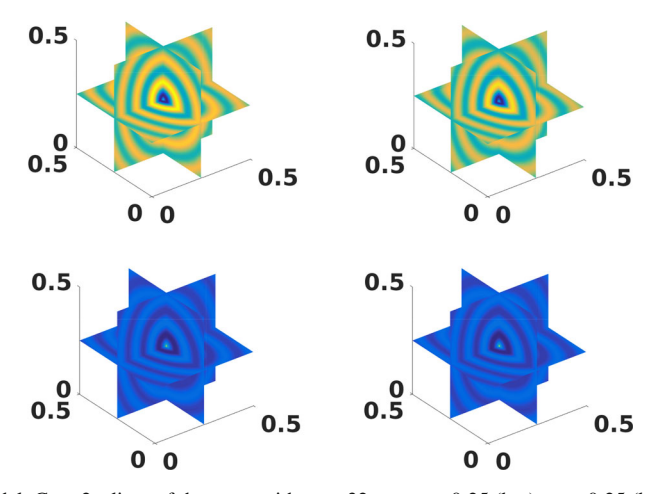


Fig. 16 3D model. Case 2: slices of the wave with $\omega=32\pi$ at x=0.25 (km), y=0.25 (km) and z=0.25 (km), respectively. Top: real part; Bottom: imaginary part. Left: U_1 ; Right: U_2 (Color figure online)

and

$$\mathbf{A}(\mathbf{r}) = \begin{pmatrix} 1 & -0.5 & -0.3 \\ -0.5 & 3 & -0.1 \\ -0.3 & -0.1 & 2 \end{pmatrix} \text{ or } \begin{pmatrix} 1 + 0.3 \sin^2(\pi x) & -0.5 + 0.1 \cos^2(\pi x) & -0.3 + 0.2 \cos^2(\pi y) \\ -0.5 + 0.1 \cos^2(\pi x) & 3 + 0.2 \sin^2(\pi y) & -0.1 - 0.1 \cos^2(\pi z) \\ -0.3 + 0.2 \cos^2(\pi y) & -0.1 - 0.1 \cos^2(\pi z) & 2 + 0.1 \sin^2(\pi z) \end{pmatrix}.$$

The source is $\mathbf{r}_0 = (0.25, 0.25, 0.25)$ (km).

References

 Abramowitz, M., Stegun, I.A.: Handbook of Mathematical Functions. Dover Publications Inc, New York (1965)



- 2. Babich, V.M.: The short wave asymptotic form of the solution for the problem of a point source in an inhomogeneous medium. USSR Comput. Math. Math. Phys. **5**(5), 247–251 (1965)
- Babuška, I.M., Sauter, S.A.: Is the pollution effect of the FEM avoidable for the Helmholtz equation considering high wave numbers? SIAM Rev. 42, 451–484 (2000)
- Benamou, J.D., Luo, S., Zhao, H.-K.: A compact upwind second order scheme for the Eikonal equation. J. Comput. Math. 28, 489–516 (2010)
- Crandall, M.G., Evans, L.C., Lions, P.-L.: Some property of viscosity solutions of Hamilton–Jacobi equations. Trans. Am. Math. Soc. 282(2), 487–502 (1984)
- Crandall, M.G., Lions, P.-L.: Viscosity solutions of Hamilton–Jacobi equations. Trans. Am. Math. Soc. 277, 1–42 (1983)
- Engquist, B., Runborg, O.: Computational high frequency wave propagation. Acta Numer. 12, 181–266 (2003)
- Fomel, S., Luo, S., Zhao, H.: Fast sweeping method for the factored eikonal equation. J. Comput. Phys. 228(17), 6440–6455 (2009)
- Glowinski, R., Leung, S., Qian, J.: Operator-splitting based fast sweeping methods for isotropic wave propagation in a moving fluid. SIAM J. Sci. Comput. 38(2), A1195

 –A1223 (2016)
- Jiang, G.S., Peng, D.: Weighted ENO schemes for Hamilton–Jacobi equations. SIAM J. Sci. Comput. 21, 2126–2143 (2000)
- Jiang, G.S., Shu, C.W.: Efficient implementation of weighted ENO schemes. J. Comput. Phys. 126, 202–228 (1996)
- Kao, C.Y., Osher, S., Qian, J.: Lax–Friedrichs sweeping schemes for static Hamilton–Jacobi equations. J. Comput. Phys. 196, 367–391 (2004)
- 13. Keller, J.B., Lewis, R.M.: Asymptotic methods for partial differential equations: the reduced wave equation and Maxwell's equations. Surv. Appl. Math. 1, 1–82 (1995)
- 14. Lions, P.-L.: Generalized Solutions of Hamilton–Jacobi Equations. Pitman, Boston (1982)
- Liu, X.D., Osher, S.J., Chan, T.: Weighted essentially nonoscillatory schemes. J. Comput. Phys. 115, 200–212 (1994)
- Lu, W., Qian, J., Burridge, R.: Babich-like ansatz for three-dimensional point-source maxwell's equations in an inhomogeneous medium at high frequencies. Multiscale Model. Simul. 14(3), 1089–1122 (2016)
- 17. Lu, W., Qian, J., Burridge, R.: Babich's expansion and the fast huygens sweeping method for the helmholtz wave equation at high frequencies. J. Comput. Phys. 313, 478–510 (2016)
- Lu, W., Qian, J., Burridge, R.: Extending babich's ansatz for point-source maxwell's equations using hadamard's method. Multiscale Model. Simul. 16(2), 727–751 (2018)
- Luo, S.: A uniformly second order fast sweeping method for Eikonal equations. J. Comput. Phys. 241, 104–117 (2013)
- Luo, S., Qian, J.: Factored singularities and high-order Lax

 –Friedrichs sweeping schemes for point-source traveltimes and amplitudes. J. Comput. Phys. 230, 4742

 –4755 (2011)
- Luo, S., Qian, J.: Fast sweeping methods for factored anisotropic Eikonal equations: multiplicative and additive factors. J. Sci. Comput. 52(2), 360–382 (2012)
- Luo, S., Qian, J., Burridge, R.: Fast Huygens sweeping methods for Helmholtz equations in inhomogeneous media in the high frequency regime. J. Comput. Phys. 270, 378–401 (2014)
- Luo, S., Qian, J., Burridge, R.: High-order factorization based high-order hybrid fast sweeping methods for point-source Eikonal equations. SIAM J. Numer. Anal. 52(1), 23–44 (2014)
- Luo, S., Qian, J., Zhao, H.: Higher-order schemes for 3D first-arrival traveltimes and amplitudes. Geophysics 77(2), T47–T56 (2012)
- Osher, S., Shu, C.-W.: High-order essentially nonoscillatory schemes for Hamilton–Jacobi equations. SIAM J. Math. Anal. 28(4), 907–922 (1991)
- Pica, A.: Fast and accurate finite-difference solutions of the 3D Eikonal equation parameterized in celerity.
 In: 67th Annual International Meeting, Society of Exploration Geophysicists, pp. 1774–1777 (1997)
- Qian, J., Lu, W., Yuan, L., Luo, S., Burridge, R.: Eulerian geometrical optics and fast Huygens sweeping methods for three-dimensional time-harmonic high-frequency Maxwell's equations in inhomogeneous media. Multiscale Model. Simul. 14(2), 595–636 (2016)
- Qian, J., Luo, S., Burridge, R.: Fast Huygens sweeping methods for multi-arrival Green's functions of Helmholtz equations in the high frequency regime. Geophysics 80(2), T91–T100 (2015)
- 29. Qian, J., Yuan, L., Liu, Y., Luo, S., Burridge, R.: Babich's expansion and high-order Eulerian asymptotics for point-source Helmholtz equations. J. Sci. Comput. 67(3), 883–908 (2016)
- Serna, S., Qian, J.: A stopping criterion for higher-order sweeping schemes for static Hamilton–Jacobi equations. J. Comput. Math. 28, 552–568 (2010)
- Zhang, L., Rector, J.W., Hoversten, G.M.: Eikonal solver in the celerity domain. Geophys. J. Int. 162, 1–8 (2005)



32. Zhang, Y.-T., Zhao, H.-K., Qian, J.: High order fast sweeping methods for static Hamilton–Jacobi equations. J. Sci. Comput. 29, 25–56 (2006)

Publisher's Note Springer Nature remains neutral with regard to jurisdictional claims in published maps and institutional affiliations.

